Effects of Threading Dislocations on AlGaN/ GaN High-Electron Mobility Transistors

Effects of Threading Dislocations on AlGaN/GaN High-Electron Mobility Transistors

Fabio Alessio Marino, *Senior Member, IEEE*, Nicolas Faralli, Tomás Palacios, *Member, IEEE*, David K. Ferry, *Fellow, IEEE*, Stephen M. Goodnick, *Fellow, IEEE*, and Marco Saraniti, *Member, IEEE*

***Abstract*—This brief aims to show the effects of threading edge dislocations on the dc and RF performance of GaN high-electron mobility transistor (HEMT) devices. A state-of-the-art high-frequency and high-power HEMT was investigated with our full-band cellular Monte Carlo (CMC) simulator, which includes the full details of the band structure and the phonon spectra. A complete characterization of the device has been performed using experimental data to calibrate the few adjustable parameters of the simulator. Thermal simulations were also carried out with commercial software in order to operate the corrections needed to model thermal effects. The approach of Weimann based on the results of Read, Bonch-Bruevich and Glasko, and Pödör was then used to model with our CMC code the dislocation effects on the transport properties of HEMT devices. Our simulations indicate that GaN HEMT performance exhibits a fairly large dependence on the density of thread dislocation defects. Furthermore, we show that a threshold concentration exists, above which a complete degradation of the device operation occurs.**

***Index Terms*—Dislocations, GaN, high-electron mobility transistor (HEMT), high-frequency, Monte Carlo, numerical simulation.**

I. Introduction

SINCE THE demonstration of the first GaN-based transistors, rapid progress has been made in their development, and novel III–N high-electron mobility transistor (HEMT) devices have been proposed. The properties of large-band-gap materials such as GaN make them ideally suited to operation at elevated temperatures because they become intrinsic at much higher temperature than narrow-band-gap materials, and sustain high current or voltage levels because they exhibit a high breakdown field. Moreover, AlGaN/GaN heterostructures do not require modulation doping, which is necessary in GaAs-based devices to create the electron gas at the heterointerface. Indeed, the discontinuity of the spontaneous polarization, due to the lack of symmetry in wurtzite crystals, induces free carriers at the interface. In addition, the piezoelectric polarization, due to the strain of the AlGaN layer, also plays an important role in increasing the density of carries in the device channel [1].

High-power operation has been achieved by GaN HEMTs in the millimeter-wave frequency range. In order to improve the high-frequency performance, the gate length L_G of the device has to be reduced [2]. This concept is well highlighted by (1), where an analytical formula to calculate the current-gain cutoff frequency f_T (see Section II-B) is reported [3] as follows:

$$f_T = \left[2\pi \int_{L_{\text{eff}}} \frac{1}{v_{\text{ave}}(x)} dx \right]^{-1} \tag{1}$$

where L_{eff} is the effective gate length and $v_{\text{ave}}(x)$ is the average velocity calculated along the channel.

However, if L_G is brought below 100–200 nm, an improvement of the frequency response can be achieved only by decreasing the barrier layer thickness and the gate length at the same time. In this case, the aspect ratio between the gate–channel distance and L_G is kept high, preventing an increase of the effective channel length with the gate length decreasing.

Nevertheless, decreasing the AlGaN barrier thickness under 15 nm causes a reduction of both density and mobility of carriers in the two-dimensional electron gas (2DEG) channel. Furthermore, at these short gate lengths, short-channel effects, such as threshold-voltage shift, soft pinchoff, and high subthreshold current, occurs due to the poor confinement of the electrons in the 2DEG channel, which reduces the modulation efficiency of the gate [4].

Recently, AlGaN/GaN HEMTs with a current-gain cutoff frequency f_T of about 180 GHz and a maximum oscillation frequency $f_{\max}$ of 230 GHz have been reported [5], [6]. This has been made possible by novel techniques, including the use of thin and high-Al-content barrier layers in order to compensate the decrease of the sheet channel charge concentration with the decrease of the barrier thickness [2]. An InGaN back barrier has also been used in order to raise the conduction band in the buffer with respect to the GaN channel, increasing the confinement of the carriers at the heterointerface [7].

However, material quality is probably still limiting the high-frequency performance, and in this brief we are going to analyze its effect in detail. Indeed, because of the lack of a suitable lattice-matched substrate, epitaxial layers of GaN can contain a high density of dislocations. So far, the substrates of choice have been sapphire (Al_2O_3) and silicon carbide (SiC), and both have shown such problems.

Manuscript received April 17, 2009; revised July 14, 2009. First published November 20, 2009; current version published December 23, 2009. This work was supported in part by the Air Force Research Laboratory under Contract FA8650-08-C-1395 and in part by the Arizona Institute for Nano-Electronics, Arizona State University, Tempe. The work of T. Palacios was supported in part by the ONR MINE MURI project. The review of this brief was arranged by Editor S. Bandyopadhyay.

F. A. Marino is with the School of Electrical, Computer and Energy Engineering, Arizona State University, Tempe, AZ 85287 USA, and also with the University of Padua, 35122 Padua, Italy (e-mail: Fabio.Marino@asu.edu).

N. Faralli, D. K. Ferry, S. M. Goodnick, and M. Saraniti are with the School of Electrical, Computer and Energy Engineering, Arizona State University, Tempe, AZ 85287 USA.

T. Palacios is with the Department of Electrical Engineering and Computer Science, Massachusetts Institute of Technology, Cambridge, MA 02139 USA.

Digital Object Identifier 10.1109/TED.2009.2035024

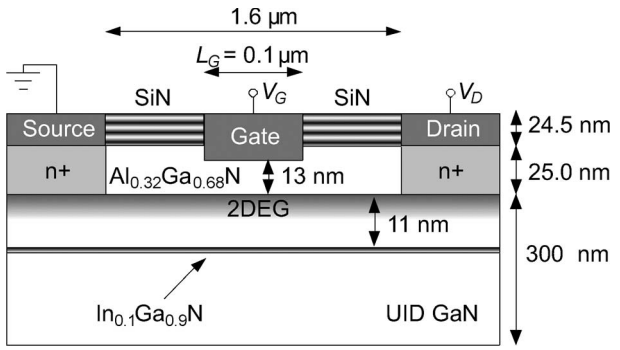

Fig. 1. Schematic cross section of the simulated InGaN back-barrier HEMT.

The threading defects are normally oriented parallel to the c-axis of the material, and their density, in GaN layers grown on a sapphire or SiC substrate, can range between 10^8 and 10^{11} cm^{-2}. Dislocations and point defects that are present in AlGaN/GaN HEMTs can become charged and act as centers of Coulomb scattering. This degrades the device performance and raises issues of device long-term reliability [8].

We first demonstrate the agreement between simulation and experiment, focusing in particular on the device layout including an InGaN back barrier proposed by Palacios et al. [6]. We then use the approach of Weimann [9], based on the results of Read [10]–[12], Bonch-Bruevich and Glasko [13], and Pödör [14], to model with cellular Monte Carlo (CMC) [15] the dislocation effects on the dc and high-frequency performance of state-of-the-art GaN HEMT power devices.

The structure of the device analyzed is described in Section II-B, where the simulation setup is summarized as well. In Section III, the theory describing the influence of threading-dislocation scattering on carrier transport is briefly discussed. The effects of dislocations on the simulated device performance are shown in Section IV. Conclusions are finally drawn in Section V.

II. GaN HEMT With InGaN Back Barrier

The layout of the device described in this brief is shown in Fig. 1 and is composed of an AlGaN/GaN heterostructure with an InGaN back barrier grown on a semi-insulating SiC substrate by metal–organic chemical vapor deposition. The heterostructure is not intentionally doped and consists, from bottom to top, of 1.5 μm of GaN, followed by 1 nm of $In_{0.1}Ga_{0.9}N$ capped by 11 nm of GaN and 25 nm of $Al_{0.32}Ga_{0.64}N$. The AlGaN layer is recessed in order to have a gate-to-channel distance of 13 nm. The source–gate and gate–drain separations are both 0.75 μm, while the gate length is set to 0.1 μm. Highly doped regions are created under the source–drain electrodes down to the GaN channel to emulate metal spikes and to control contact resistances.

As mentioned in the Introduction, the presence of the InGaN layer enhances the confinement of the electrons in the channel. In fact, the large polarization-induced electric field in the InGaN layer raises the conduction-band edge of the GaN buffer with respect to the GaN channel, creating a potential barrier against carrier diffusion in the bulk layer. This property is shown in Fig. 2, showing the carrier distribution (black points) at $V_{\rm GS} = 0$ V and $V_{\rm DS} = 6$ V, superimposed on the conduction-band profile of the simulated device.

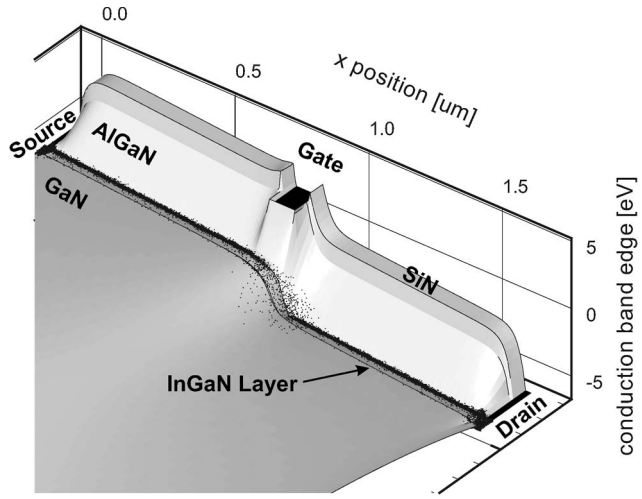

Fig. 2. Conduction-band profile and carrier distribution (black points) corresponding to biases of 0 V on the gate and 6 V on the drain.

More details on that device can be found in [6], where all the characteristics of the sample used to obtain the experimental data are reported.

A. Simulation Setup

To account for the large polarization discontinuity that is present at the AlGaN/GaN and InGaN/GaN heterointerfaces, explicit sheets of charge were set at these interfaces following the formulation of Ambacher et al. [16].

The large polarization-induced charge at the AlGaN barrier surface would completely deplete the channel of electrons if it were not (partially or completely) compensated by fixed charges or surface traps [17]. In this brief, we assumed that it is partially compensated by fixed positive charge. More precisely, the charge concentration that was set at the SiN/AlGaN interface was -0.011 C/m^{-2}, whereas at the AlGaN/GaN heterointerface, we used 0.0276 C/m^{-2}.

Fig. 3 shows a comparison of the simulated (dashed lines) and measured (dots) I_D–V_D characteristics of the HEMT. As it can be seen, the simulation results are in very good agreement with the experimental data in the low-drain-bias region. However, the simulated current is increasingly higher than the experimental one with increasing drain and gate biases. This discrepancy is due to self-heating effects under high-power operation.

To account for these effects, thermal simulations were carried out with the commercial simulation program Sentaurus [18]. The thermodynamic (or nonisothermal) model [19] implemented in this software tool extends the drift–diffusion approach to account for electrothermal effects, under the assumption that the charge carriers are in thermal equilibrium with the lattice. Therefore, the carrier and lattice temperatures are described by a single temperature.

The temperature distribution within the device has been computed at $V_{\rm GS} = 0$ and 1 V for different drain biases. Fig. 4

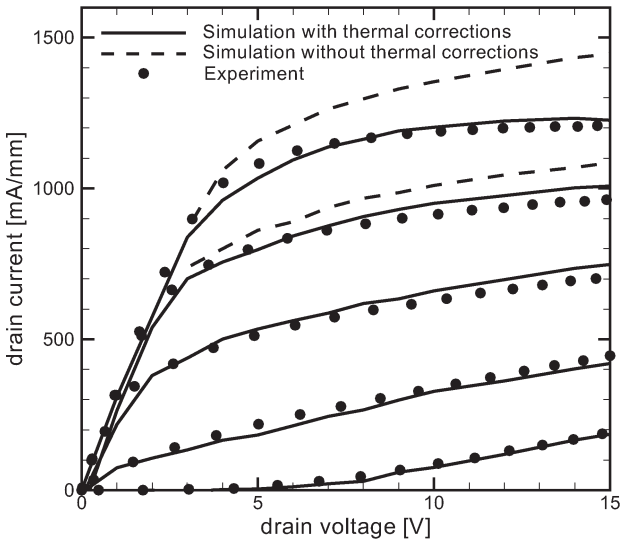

Fig. 3. Comparison of (lines) simulated and (dots) measured I_D–V_D characteristics of the HEMT. The dashed lines represent the CMC results obtained with the thermal corrections (see the text). The gate voltage V_G is ranged between 1 and -3 V with a bias step of $\Delta V_G = 1$ V.

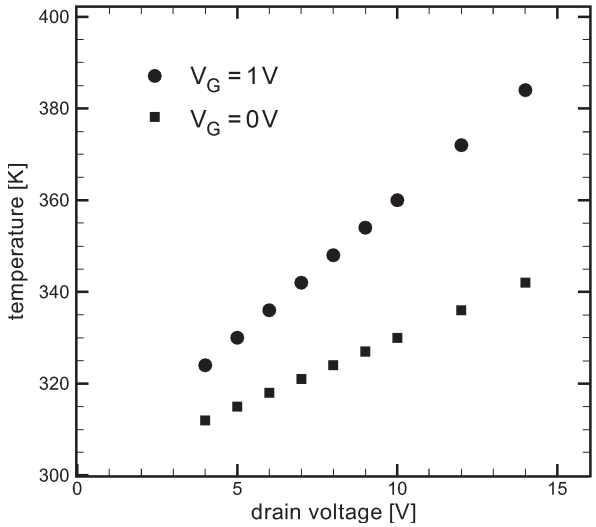

Fig. 4. Temperature calibration curves corresponding to biases of 0 and 1 V on the gate.

shows the temperature calibration curves in the channel for $V_{\rm GS} = 0$ V and $V_{\rm GS} = 1$ V. The results obtained by this analysis were used to set the number of phonons in the scattering tables used for CMC simulations.

As can be seen in Fig. 3, the thermally corrected simulation results (solid lines) are in full agreement with the experimental data.

Concerning the simulation parameters, the electronic structure was computed with a local empirical pseudopotential method [20]. The phonon spectra were computed with the Keating approach [21]. Nonpolar scattering rates were tabulated in momentum space with an isotropic deformation potential. Polar scattering was computed by the usual Fröhlich expression, as described in [15]. Dislocation scattering is discussed in detail in Section III. As customary with our CMC simulations, a different inhomogeneous tensor-product grid was used for

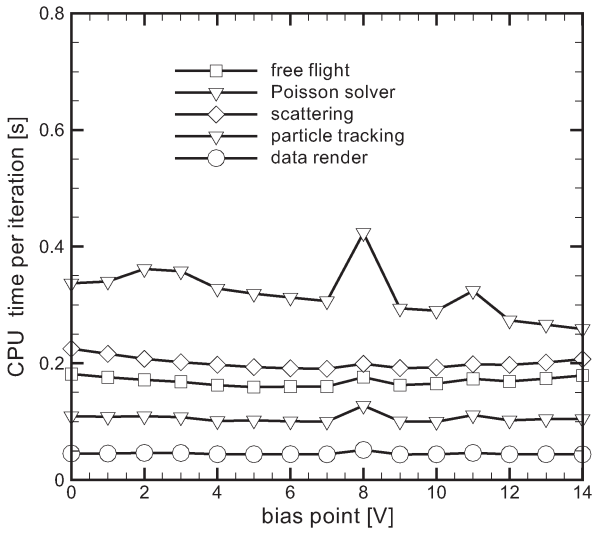

Fig. 5. Performance of the algorithmic components of the simulation code at different bias points.

each band in the first Brillouin zone (BZ1) of the momentum space. All energies were tabulated, meaning that no analytical approximation of the electronic dispersion and of the phonon spectra were used in any subregion of BZ1.

The position space of the device was represented on a 178×100 inhomogeneous tensor-product grid where Poisson's equation was solved. We used an iterative version of the multigrid Poisson solver [22] with relaxation for both pre- and postsmoothing [23]. The Poisson solver was iterated until the normalized maximum difference between two subsequent solutions was smaller than 10^{-5}. Because of the irregular nature of the grid, the charge assignment and field interpolation scheme was nearest grid point [24].

Simulations were run for different dislocation concentrations in the range of $10^8 - 10^{12}$ cm^{-2}. Accordingly, the Poisson time step was in the range of 0.3–2.5 fs, while the (constant) free-flight time step [25] was set in the range of 0.03–0.2 fs. Each bias point was obtained starting from the carrier distribution of the previous one, and each run lasted for 6 ps of simulated time, with ensemble and time averages performed during the last 2 ps. The first point was run for 40 ps, and averages were performed in the last 6 ps. The carrier (electron) population was represented by 50 000 superparticles.

The (scalar) runs were performed on 64-b processors running at a frequency of 2.8 GHz, and the transition table was not larger than 3TB. The performance of the simulation code is shown in Fig. 5, where the CPU time per iteration for each main algorithmic component of the code is listed for the set of bias points corresponding to the $V_{\rm GS} = 0 -$ V curve in Fig. 3.

B. RF Analysis of AlGaN/GaN HEMT

Several figures of merit are often used to evaluate the performance of microwave devices [4]. The most important metrics for the frequency performance of microwave transistors are the cutoff frequency f_T and the maximum frequency of oscillation $f_{\max}$ [26]. The cutoff frequency is related to the short-circuit current gain h_{21}, which is defined as the ratio of the

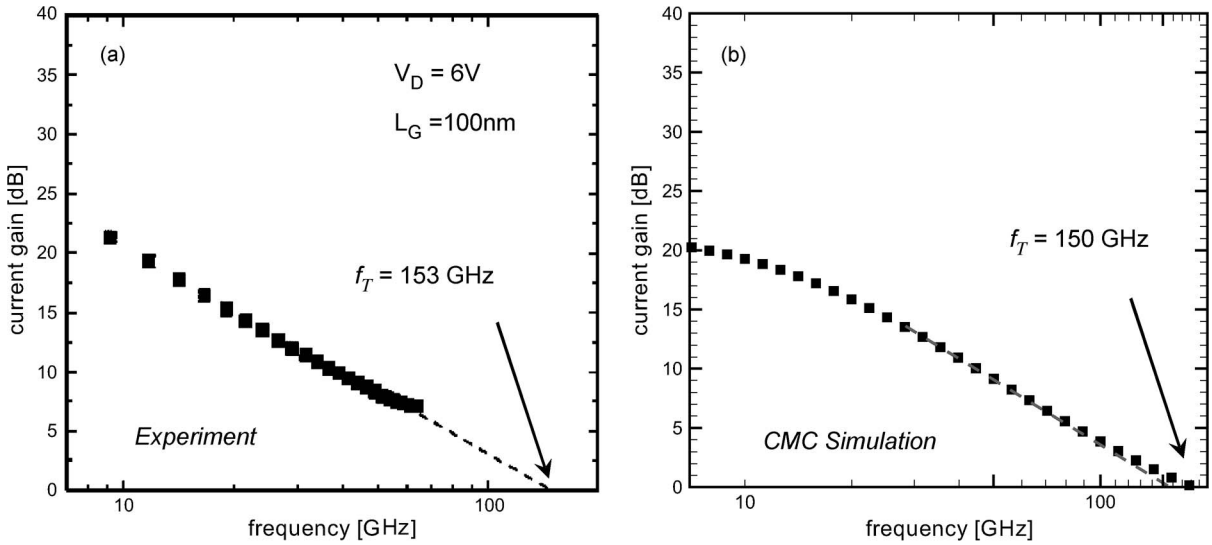

Fig. 6. Current gain as a function of frequency obtained by (a) experimental measurement and (b) CMC simulation.

small-signal output current to the small-signal input current of the device when the output terminals are shorted [4]. The maximum frequency of oscillation is the frequency at which the transistor still provides a power gain.

The basic idea of the small-signal frequency, or RF, analysis consists of applying a small perturbation to one electrode of the device in steady state while keeping all other parameters constant. The small-signal parameters can then be derived from the recorded transient response. The response in the transient regime is a function of device characteristics, such as geometry, doping profile, transport property in the device, and steady-state operating point (i.e., the dc component of $V_{\rm DS}$ and $V_{\rm GS}$) [27].

In our study, the operating point for the RF analysis ($V_{\rm GS} = 0$ V and $V_{\rm DS} = 6$ V) has been chosen in order to compare the simulation results with the experimental data [6]. The current gain as a function of frequency is shown in Fig. 6. The right plot, representing the simulation results, is obtained by the Fourier decomposition method [4], a straightforward technique, where perturbation is a small step voltage applied to one electrode of the device in steady state. The gate and drain step amplitudes used were 0.5 and 1 V, respectively. This figure shows that a cutoff frequency f_T of 150 GHz has been found, which matches to the experimental findings [6].

C. Johnson Figure of Merit

In general, materials like GaN have been considered to have desirable properties for high-power applications due to their large band gap and high thermal conductivity. One well-known figure of merit for this is the *Johnson figure of merit* [28]

$$FoM_{\rm Johnson} = \frac{v_{\rm sat} E_{\rm BD}}{2\pi} \tag{2}$$

where $v_{\rm sat}$ is the saturation velocity and $E_{\rm BD}$ is the electric field at which impact ionization starts to cause breakdown. Unfortunately, this is a difficult figure of merit to apply as the saturation velocity and breakdown field are intrinsic properties of a device. While they can easily be found in simulation, they are more difficult to determine experimentally. However, these can be connected to microwave measurements in a meaningful manner. Generally, the cutoff frequency f_T is related to the effective saturation velocity through a well-known formula

$$f_T = \frac{v_{\rm sat}}{2\pi L_G} \tag{3}$$

where L_G is the gate length (or effective gate length to be more precise [3]). We also find from detailed simulations that the field under the gate varies almost linearly over the length of the effective gate. Breakdown usually occurs near the drain end of the gate, where the highest field occurs. Because there is also a potential drop across the space between the gate and the contacts, we can write the breakdown voltage in terms of the breakdown field as

$$V_{\rm BD} = \alpha \frac{E_{\rm BD} L_G}{2} \tag{4}$$

where α is an adjustable parameter that relates the voltage drop across the gate to the total voltage applied to the device. Hence, we can rewrite the figure of merit in terms of these experimentally determined parameters as

$$FoM_{\rm Johnson} = \frac{1}{2\pi}(2\pi L_G f_T)\frac{2V_{\rm BD}}{\alpha L_G} = \frac{2}{\alpha} f_T V_{\rm BD}. \tag{5}$$

The α parameter can be extracted directly from the simulations using (4) and calculating the breakdown voltage as integral of the field across the channel when impact ionization starts.

Using a value that was previously published for GaN for (2) [29] and values found in simulations of GaN HEMTs, we find that α takes a value around 1.25, but this factor could actually be ignored without much loss of relevance of the figure of merit. Following (5) and assuming a breakdown voltage of 80 V [30], a $FoM_{\rm Johnson}$ around 20×10^{12} V/s was found for the HEMT device analyzed in this brief. After showing that our CMC simulation agrees well with the experiment, we can now examine the role of dislocations.

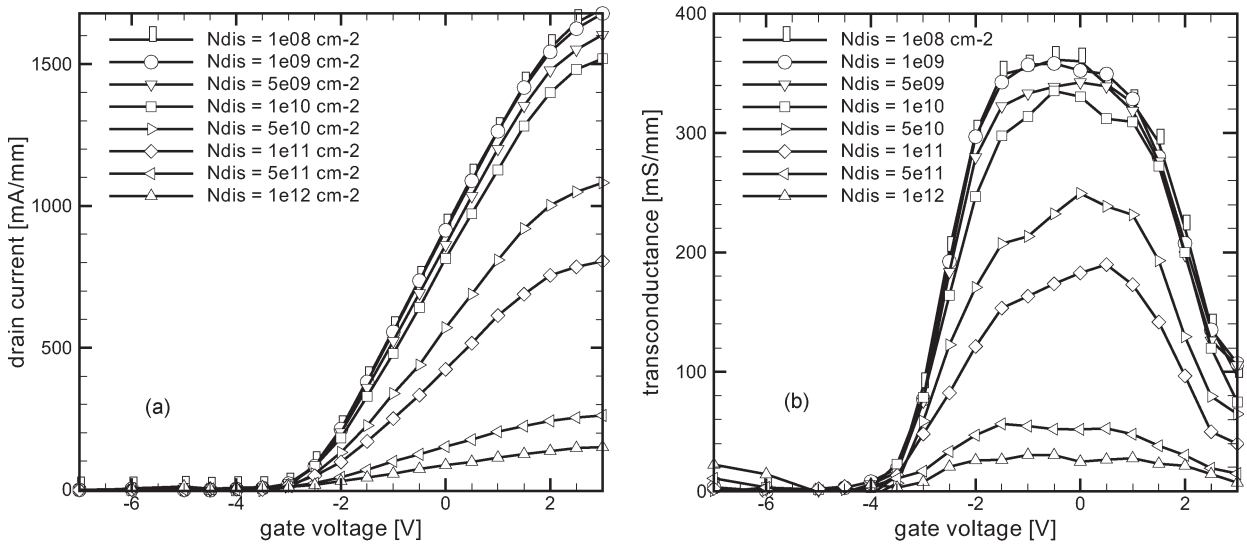

Fig. 7. (a) I_D–V_G characteristics and (b) transconductance-versus-gate-voltage curves as obtained by device simulations at values of threading-edge-dislocation density ranging from $N_{\rm dis} = 10^8$ to 10^{12} cm^{-2}.

III. Dislocation Scattering

GaN layers grown on sapphire or silicon carbide suffer from biaxial strain due to the quite-large lattice mismatches between materials, i.e., 2.5% and 3.6% at 298 K, respectively [31]. These mismatches, together with the large difference in the thermal expansion coefficient of the adjacent materials, result in threading edge and screw dislocations with typical concentrations in the range of 10^8-10^{11} cm^{-2} [8]. It has been shown [32] that the dislocation lines are negatively charged and therefore act as lines of Coulomb scattering centers for conduction electrons.

Read [10]–[12] and Bonch-Bruevich and Glasko [13] calculated the occupation statistics of dislocation acceptor centers and the potential due to a vertical line of charges. Some years later, Pödör obtained a momentum relaxation rate and mobility after averaging over energy [14]. Weimann et al. [9] employed this relaxation rate and obtained a good agreement with the measured Hall mobility in wurtzite GaN. The approach of Weimann et al. is used in this brief.

The scattering due to dislocation-line charges is 2-D because only electrons moving perpendicular to the dislocation line can be scattered. The scattering probability can therefore be expressed as a function of the 2-D perpendicular momentum $\vec{k}_\perp$ and the parallel component k_z that is conserved through the scattering process [32].

Using the Weimann approach, the scattering probability for an electron with 3-D initial momentum $(\vec{k}_\perp, k_z)$ to a small region $\Omega_{\vec{k}'_\perp,k_z}$ centered in $(\vec{k}'_\perp, k_z)$, if $N_{\rm dis}$ is the number of threading edge dislocations and f is the fraction of filled traps, can be expressed as follows:

$$P^{\rm dis}\left(\vec{k}_\perp, k_z, \Omega_{\vec{k}'_\perp,k_z}\right) = \frac{2\pi}{\hbar}\frac{N_{\rm dis}e^4\lambda^4 f^2}{\epsilon^2 c^2(1+q^2\lambda^2)^2} \times \left|I\left(\vec{k}_\perp, k_z, \vec{k}'_\perp, k'_z\right)\right|^2 D_\perp\left(E', \Omega_{\vec{k}'_\perp,k_z}\right) \quad (6)$$

where $\hbar$ is the reduced Plank's constant, e is the electron charge, ϵ is the semiconductor static dielectric constant, c is the lattice parameter along the (0001) direction, $\vec{q} = \vec{k}_\perp - \vec{k}'_\perp$, and λ is the screening length. I is the overlap integral, while $D_\perp$ represents the 2-D density of states perpendicular to the c-axis. The (generally different) band indices of the initial and final wave vectors have been omitted to simplify the notation. In agreement with [9], in bulk wurtzite GaN, the fraction of filled traps increases with the dislocations and the free-carrier density. Because, in an HEMT device, such as the one analyzed here, most of the electrons are confined in the AlGaN/GaN heterointerface, where a large quantity of carriers are present, a filling factor f that is equal to one has been chosen for our study.

IV. Effect of Dislocations on Device Performance

In order to obtain a quantitative insight about the effects of dislocations on HEMTs' performance, the rate expressed in (6) was implemented in our code and used to perform the dc and frequency analysis at different dislocation concentrations.

A. DC Analysis

Various degradation modes related to the mobility reduction caused by dislocation scattering have been identified, including the lowering of the drain current and the transconductance peak value. Both of these effects can be seen in Fig. 7, where the I_D–V_G characteristics and the transconductance curves are reported as obtained by simulations at values of threading-edge-dislocation density in the range of $N_{\rm dis} = 10^8$–10^{12} cm^{-2}.

As it can be seen, when $N_{\rm dis}$ ranges between 10^8 and 10^{10} cm^{-2}, the threading defects do not significantly affect the device behavior, which shows a quite-high drain current (< 1500 mA/mm). Also, the transconductance peak value is larger than 350 mS/mm and is almost unchanged by defect scattering. In particular, if $N_{\rm dis} < 10^9$ cm^{-2}, the scattering from dislocations is negligible with respect to the other scattering mechanisms.

However, when the dislocation concentration exceeds the "threshold" value of 10^{10} cm^{-2}, the transport properties start

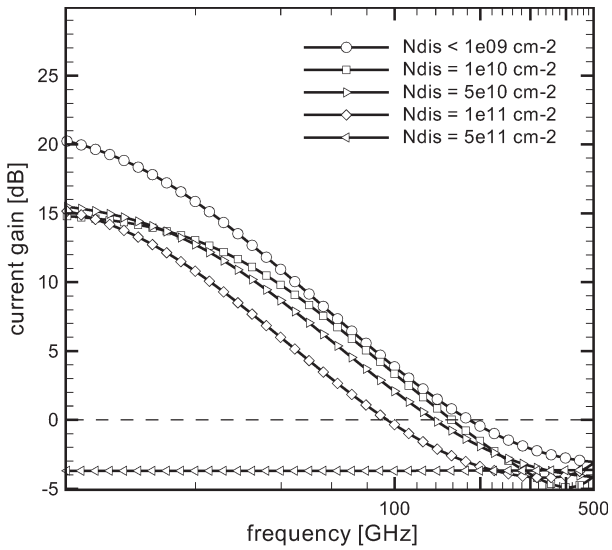

Fig. 8. Current gain as a function of frequency for different densities of threading edge dislocations.

to degrade significantly, and both drain current and transconductance decrease by a factor of two or more. When $N_{\rm dis}$ is increased above 10^{11} cm^{-2}, the device is completely compromised and ceases to work as a transistor.

B. Frequency Analysis

The main results of RF analysis are shown in Fig. 8, where the current gain versus frequency is plotted for different values of dislocation density. As in Fig. 2, the operating point ($V_{\rm GS} = 0$ V, $V_{\rm DS} = 6$ V) is chosen.

As it can be seen, the cutoff frequency exhibits fairly large changes with the dislocation density, ranging from 150 GHz, corresponding to a concentration of $N_{\rm dis} = 10^8 - 10^9$ cm^{-2}, to 90 GHz, for $N_{\rm dis} = 10^{11}$ cm^{-2}.

Also, in this case, the device performance is considerably compromised above the critical concentration of $N_{\rm dis} = 10^{11}$ cm^{-2}. Beyond this value, in fact, the current gain is almost zero for all frequencies, and a cutoff frequency is not identifiable.

V. Conclusion

In this brief, the results of the first complete full-band study on the influence of threading-dislocation scattering on carrier transport in GaN HEMT devices have been presented.

The scattering rate of Weimann, based on the first-principles theory of Read, Bonch-Bruevich and Glasko, and Pödör, was used to implement the threading-dislocation scattering in our full-band CMC simulation code, which includes the full details of the band structure and the phonon spectra.

Thermal simulations were performed with commercial software in order to determine the corrections needed to model thermal effects with our particle-based CMC simulator.

Our simulations indicate that the GaN HEMT device performance exhibits a fairly large dependence on the density of threading-dislocation defects. Various degradation modes related to defect scattering have been identified, including the lowering of the drain current and the transconductance peak value. More in detail, we have observed that, when the dislocation concentration ranges between 10^8 and 10^{10} cm^{-2}, the threading-dislocation defects do not significantly affect the dc behavior of the device. In particular, if $N_{\rm dis} < 10^9$ cm^{-2}, the scattering from dislocations is negligible with respect to the other scattering mechanisms. However, if the dislocation concentration exceeds a value of 10^{10} cm^{-2}, the transport properties start to degrade seriously, and both drain current and transconductance decrease by a factor of two or more. An analogous situation holds for the frequency performance that is sensibly related to material quality, and the only difference in this case is that the degradation is more progressive with an increasing number of crystal defects.

We have also shown that, if the number of dislocations exceeds the critical concentration of $N_{\rm dis} = 10^{11}$ cm^{-2}, the device transport properties and, therefore, dc and RF device performance are completely compromised.

References

[1] O. Ambacher, J. Smart, J. R. Shealy, N. G. Weimann, M. M. K. Chu, W. J. Schaff, L. F. Eastman, R. Dimitrov, L. Wittmer, M. Stutzmann, W. Rieger, and J. Hilsenbeck, "Two-dimensional electron gases induced by spontaneous and piezoelectric polarization charges in N- and Ga-face AlGaN/GaN heterostructures," *J. Appl. Phys.*, vol. 85, no. 6, pp. 323–3222, 1999.

[2] M. Higashiwaki and T. Matsui, "AlGaN/GaN heterostructure field-effect transistors with current gain cut-off frequency of 152 GHz on sapphire substrates," *Jpn. J. Appl. Phys.*, vol. 44, no. 16, pp. L475–L478, Apr. 2005.

[3] R. Akis, J. Ayubi-Moak, N. Faralli, D. K. Ferry, S. M. Goodnick, and M. Saraniti, "The upper limit of the cutoff frequency in ultrashort gate-length InGaAs/InAlAs HEMTs: A new definition of effective gate length," *IEEE Electron Device Lett.*, vol. 29, no. 4, pp. 306–308, Apr. 2008.

[4] F. Schwierz and J. Liou, *Modern Microwave Transistors: Theory, Design, and Performance*. New York: Wiley, 2003.

[5] M. Higashiwaki and T. Matsui, "30-nm-gate AlGaN/GaN heterostructure field-effect transistors with a current-gain cutoff frequency of 181 GHz," *Jpn. J. Appl. Phys.*, vol. 45, no. 42, pp. L1 111–L1 113, Oct. 2006.

[6] T. Palacios, A. Chakraborty, S. Heikman, S. Keller, S. P. DenBaars, and U. K. Mishra, "AlGaN/GaN high electron mobility transistors with InGaN back-barriers," *IEEE Electron Device Lett.*, vol. 27, no. 1, pp. 13–15, Jan. 2006.

[7] G. Simin, X. Hu, A. Tarakji, J. Zhang, A. Koudymov, S. Saygi, J. Yang, A. Khan, M. S. Shur, and R. Gaska, "AlGaN/InGaN/GaN double heterostructure field-effect transistor," *Jpn. J. Appl. Phys.*, vol. 40, no. 11A, pp. L1 142–L1 144, Nov. 2001.

[8] R. P. Joshi, S. Viswanadha, B. Jogai, P. Shah, and R. D. del Rosario, "Analysis of dislocation scattering on electron mobility in GaN high electron mobility transistors," *J. Appl. Phys.*, vol. 93, no. 12, pp. 10 046–10 052, Jun. 2003.

[9] N. Weimann, L. Eastman, D. Doppalapudi, H. Ng, and T. Moustakas, "Scattering of electrons at threading dislocations in GaN," *J. Appl. Phys.*, vol. 83, no. 7, pp. 3656–3659, Apr. 1998.

[10] W. T. Read, "Theory of dislocations in germanium," *Philos. Mag.*, vol. 45, no. 367, pp. 775–796, Aug. 1954.

[11] W. T. Read, "Statistics of the occupation of dislocation acceptor centres," *Philos. Mag.*, vol. 45, no. 370, pp. 1119–1128, Nov. 1954.

[12] W. T. Read, "Scattering of electrons by charged dislocations in semiconductors," *Philos. Mag.*, vol. 46, no. 373, pp. 111–131, Feb. 1955.

[13] V. Bonch-Bruevich and V. Glasko, "The theory of electron states connected with dislocations. I. Linear dislocations," *Fiz. Tverd. Tela*, vol. 3, p. 36, Jun. 1961.

[14] B. Podor, "Electron mobility in plastically deformed germanium," *Phys. Stat. Sol. B*, vol. 16, no. 2, pp. K167–K169, Jul. 1966.

[15] M. Saraniti and S. Goodnick, "Hybrid full-band cellular automaton/Monte Carlo approach for fast simulation of charge transport in semiconductors," *IEEE Trans. Electron Devices*, vol. 47, no. 10, pp. 1909–1915, Oct. 2000.

[16] O. Ambacher, J. Majewski, C. Miskys, A. Link, M. Hermann, M. Eickhoff, M. Stutzmann, F. Bernardini, V. Fiorentini, V. Tilak, B. Schaff, and L. Eastman, "Pyroelectric properties of Al(In)GaN/GaN hetero- and quantum well structures," *J. Phys., Condens. Matter*, vol. 14, no. 13, pp. 3399–3434, Mar. 2002.
[17] J. P. Ibbetson, P. T. Fini, K. D. Ness, S. P. DenBaars, J. S. Speck, and U. K. Mishra, "Polarization effects, surface states, and the source of electrons in AlGaN/GaN heterostructure field effect transistors," *Appl. Phys. Lett.*, vol. 77, no. 2, pp. 250–252, Jul. 2000.
[18] Synopsys, Inc., *Sentaurus Device User's Manual*, Mountain View, CA, 2008. Ver. y-2008.
[19] G. Wachutka, "An extended thermodynamic model for the simultaneous simulation of the thermal and electrical behavior of semiconductor devices," in *Proc. 6th Int. Conf. NASECODE*, Jul. 1989, vol. 5, pp. 409–414.
[20] J. Chelikowsky and M. Cohen, "Nonlocal pseudopotential calculations for the electronic structure of eleven diamond and zinc-blend semiconductors," *Phys. Rev. B, Condens. Matter*, vol. 14, no. 2, pp. 556–582, Jul. 1976.
[21] P. Keating, "Effect of invariance requirements on the elastic strain energy of crystal with application on diamond structure," *Phys. Rev. Lett.*, vol. 145, no. 2, pp. 637–645, May 1966.
[22] W. Hackbush, *Multi-Grid Methods and Applications*. Berlin, Germany: Springer-Verlag, 1985.
[23] M. Saraniti, A. Rein, G. Zandler, P. Vogl, and P. Lugli, "An efficient multigrid Poisson solver for device simulations," *IEEE Trans. Comput.-Aided Design Integr. Circuits Syst.*, vol. 15, no. 2, pp. 141–150, Feb. 1996.
[24] R. Hockney and J. Eastwood, *Computer Simulation Using Particles*. Bristol, U.K.: Adam Hilger, 1988.
[25] M. Fischetti and S. Laux, "Monte Carlo analysis of electron transport in small semiconductor devices including band-structure and space-charge effects," *Phys. Rev. B, Condens. Matter*, vol. 38, no. 14, pp. 9721–9745, Nov. 1988.
[26] K. F. Brennan and A. S. Brown, *Theory of Modern Electronic Semiconductor Devices*. New York: Wiley, 2002.
[27] S. Yamakawa, "Transport modeling in GaN materials and devices based on full-band cellular Monte Carlo simulation," Ph.D. dissertation, Arizona State Univ., Tempe, AZ, 2003.
[28] A. Johnson, "Physical limitations on frequency and power parameters of transistors," *RCA Rev.*, vol. 26, pp. 163–177, Jun. 1965.
[29] P. Das and D. Ferry, "Hot electron microwave conductivity of wide bandgap semiconductors," *Jpn. J. Appl. Phys.*, vol. 19, pp. 851–855, 1976.
[30] T. Palacios, Y. Dora, A. Chakraborty, C. Sanabria, S. Keller, S. P. DenBaars, and U. K. Mishra, "Optimization of AlGaN/GaN HEMTs for high frequency operation," *Phys. Stat. Sol. A*, vol. 203, no. 7, pp. 1845–1850, May 2006.
[31] M. Manasreh, *III-V Nitride Semiconductors: Defects and Structural Properties*. Amsterdam, The Netherlands: Elsevier, 2000.
[32] M. N. Gurusinghe and T. G. Andersson, "Mobility in epitaxial GaN: Limitations of free-electron concentration due to dislocations and compensation," *Phys. Rev. B, Condens. Matter*, vol. 67, no. 23, p. 235 208, Jun. 2003.

Fabio Alessio Marino (SM'06) received the M.S. degree (*summa cum laude*) in electronic engineering from the University of Padua, Padua, Italy, in 2006. He is currently working toward the Ph.D. degree (dual-degree program) in electrical engineering in the School of Electrical, Computer and Energy Engineering, Arizona State University, Tempe, and the University of Padua.

While completing his B.E. and M.S. programs, he developed a static logic family and a novel CMOS technology for the realization of high-density integrated circuits. Both technologies have been patented. In August 2008, he joined the School of Electrical Computer and Energy Engineering, Arizona State University, as a Ph.D. candidate focusing his work on Monte Carlo simulation of high-frequency devices such as gallium nitride HEMTs. He is an author or a coauthor of several scientific papers in international journals, conference proceedings (one of which received the Best Paper Award), and invited talks and is a holder of three approved and one pending patents.

Nicolas Faralli received the M.S. degree in computer systems engineering from the Illinois Institute of Technology, Chicago, in 2004, the M.E. degree in electrical and computer engineering from the Ecole Nationale Superieure de l'Electronique et de ses Applications, Cergy, France, in 2004, and the Ph.D. degree from Arizona State University, Tempe, in 2009.

He is currently a Postdoctoral Associate at the School of Electrical, Computer and Energy Engineering, Arizona State University. His research activity focuses mainly on the frequency analysis of heterojunction devices via full-band Monte Carlo simulations.

Tomás Palacios (S'98–M'06) received the M.S. and Ph.D. degrees in electrical engineering from the University of California, Santa Barbara (UCSB), in 2004 and 2006, respectively.

In 1997, he joined the Institute for Systems based on Optoelectronics and Microtechnology, Spain. There, he worked on technology research, ultraviolet photodetectors, surface-acoustic-wave filters, and high-electron mobility transistors. In 2000, he was with the Microelectronics Group, European Organization for Nuclear Research (CERN, Geneva, Switzerland), where he collaborated in the design of new Si transistors for radiation-hardened and low-noise electronics. In 2002, he joined Prof. Mishra's group at UCSB, where he developed new transistors based on nitrides for millimeter-wave applications and established the state of the art in high-frequency and high-power applications. He joined the Department of Electrical Engineering and Computer Science, MIT, in September 2006 as an Assistant Professor and a member of the Microsystems Technology Laboratory. His research interests include the design, processing, and characterization of new transistors based on wide-band-gap semiconductors for power amplification and digital applications beyond 100 GHz. He is also an author or a coauthor of more than 70 scientific papers in international journals and conferences, one book chapter, and several invited talks.

Dr. Palacios' work has been recognized by multiple awards, including the NFS CAREER Award, the ONR Young Investigator Award, the DARPA Young Faculty Award, the Young Researcher Award at the Sixth International Conference on Nitride Semiconductors, the Best Student Paper Award at the 36th Device Research Conference, and the UCSB Lancaster Dissertation Award.

David K. Ferry (S'61–M'62–SM'72–F'87) received the B.S.E.E and M.S.E.E. degrees from Texas Tech University, Lubbock, in 1962 and 1963, respectively, and the Ph.D. degree from the University of Texas, Austin, in 1966.

He then spent an NSF Postdoctoral Fellowship in Vienna, Austria. He was a Member of the Faculty with Texas Tech University from 1967 to 1973 and then joined the Office of Naval Research, Washington, DC. From 1977 to 1983, he was with Colorado State University, Fort Collins, and then joined Arizona State University, Tempe, where he was the Director of the Center for Solid State Electronics Research (1983–1989), the Chair of Electrical Engineering (1989–1992), and the Associate Dean for Research (1993–1995) and is currently with the School of Electrical, Computer and Energy Engineering. He was selected as one of the first Regents' Professors at Arizona State University in 1998. He has published more than 600 articles, books, book chapters, and conference publications. His work addresses transport physics and model of quantum effects in submicrometer semiconductor devices and electron-beam lithography for ultra-submicrometer quantum functional devices.

Dr. Ferry is a Fellow of the American Physical Society. He received the IEEE Cledo Brunetti Award for advances in nanoelectronics.

Stephen M. Goodnick (M'88–SM'91–F'04) received the B.S. degree in engineering science from Trinity University, San Antonio, TX, in 1977 and the M.S. and Ph.D. degrees in electrical engineering from Colorado State University, Fort Collins, in 1979 and 1983, respectively.

He was an Alexander von Humboldt Fellow with the Technical University of Munich, Munich, Germany, and the University of Modena, Modena, Italy, in 1985 and 1986, respectively. He was a Faculty Member from 1986 to 1997 with the Department of Electrical and Computer Engineering, Oregon State University, Corvallis, and was the Chair and a Professor of electrical engineering with Arizona State University, Tempe, from 1996 to 2005. He was the Deputy Dean and Director of Nanoelectronics for the Ira A. Fulton School of Engineering, Arizona State University, during 2005–2006, where he was appointed as Associate Vice President for Research in 2006. He has coauthored over 165 journal articles, books, and book chapters related to transport in semiconductor devices and nanostructures.

Dr. Goodnick was the President of the Electrical and Computer Engineering Department Heads Association in 2003–2004 and was the Program Chair for the Fourth IEEE Conference on Nanotechnology in Munich in August 2004.

Marco Saraniti (M'98) received the Ph.D. degree from the Walter Schottky Institute, Technical University of Munich, Munich, Germany, in 1996.

After graduating in 1996, he was a Faculty Research Associate with the Department of Electrical Engineering, Arizona State University, Tempe, for two years. In 1998, he moved to Illinois Institute of Technology, Chicago, where he was awarded the tenure in 2004 and achieved the position of Associate Professor. In 2007, he became a Professor with the School of Electrical, Computer and Energy Engineering, Arizona State University. His current research activity focuses mainly on computational electronics applied to the simulation of semiconductor devices and biological structures. He is an author or a coauthor of more than 80 publications, four book chapters, and four technical reports. His recent scientific work covers the following fields: 1) development of Monte Carlo and cellular automaton techniques for 2-D and 3-D physical simulation of semiconductor devices; 2) simulation and engineering of semiconductor devices; and 3) development of numerical methods for the modeling and simulation of membrane proteins.